Time-Resolved Photoluminescence Characteristics of Subnanometer ZnO Clusters Confined in the Micropores of Zeolites

Jianying Shi, Jun Chen, Zhaochi Feng, Tao Chen, Xiuli Wang, Pinliang Ying, and Can Li*

State Key Laboratory of Catalysis, Dalian Institute of Chemical Physics, Chinese Academy of Sciences, Dalian 116023, China

Received: January 20, 2006; In Final Form: October 18, 2006

Subnanometric ZnO clusters confined in different micropore zeolites are studied by steady-state and nanosecond time-resolved photoluminescence (PL) spectroscopy. The microsecond-scale lifetime is observed at room temperature for ZnO clusters confined in zeolites, which is significantly different from that of macrocrystalline ZnO on the external surface of zeolites. The dependence of luminescence lifetime on the amount of ZnO in zeolites indicates that the electron−phonon interactions between the ZnO clusters and the zeolite host significantly affect the dynamic relaxation process of ZnO clusters. The long lifetime luminescence of ZnO clusters can be achieved by weakening the coupling of electronic transition to zeolites host phonons. The similar long-lived luminescence is obtained when dispersing ZnO clusters into the porous SiO_2. It is suggested that encapsulating the semiconductor cluster in the porous support is a possible way to inhibit or to retard the electron−hole recombination.

Introduction

An understanding of charge carrier dynamics in semiconductor material is of fundamental interest and important particularly for photocatalysis[1] and solar energy conversion.[2,3] Time-resolved photoluminescence (TRPL) is a nondestructive and powerful technique commonly used for the optical characterization of semiconductors. The carrier or exciton lifetime, an important parameter related to material quality and device performance, can be measured by TRPL spectroscopy. Semiconductor ZnO has drawn considerable attention because of its promising applications in solar cell, photocatalysis, light emission, gas sensor, and other optical devices.[4−6] The relaxation dynamics of zinc oxide in various forms, such as film,[7] nanopowder,[8] quantized ZnO colloids,[9−12] nanorods,[13] and nanoneedles,[14] has been studied by TRPL spectroscopy or ultrafast pump−probe absorption spectroscopy.[7−14] The steady-state PL spectra of ZnO in various forms are mainly composed of a narrow UV emission band and a broader visible luminescence band. The UV luminescence band at about 380 nm ascribed to the exciton emission is rapidly decayed on the order of several tens to hundreds of picoseconds.[13−15] The lifetimes of the visible luminescence band change from several tens to thousands nanoseconds for various ZnO forms.[7−12,16]

Much of research has been focused on the nanometer or micrometer ZnO material; however, little attention is paid to the subnanometric ZnO clusters. The well-defined and well-ordered pores of zeolites can be used to accommodate semiconductor clusters, and the size and configuration of semiconductor clusters can be tailored using different zeolites.[17−24] We have employed micropores of zeolites as host and prepared stable subnanometric ZnO clusters[25] that display special photophysical and photochemical properties for the quantum confinement effect. The ZnO clusters confined in zeolite exhibit the purple luminescence band (centered at 410−445 nm) with high quantum efficiency and the absorption onset is below 265 nm.[25] In the present paper, we further study the relaxation dynamics of ZnO clusters confined in zeolites by time-resolved photoluminescence spectroscopy. Two types of microporous zeolites, HZSM-5 (pore diameter ∼ 5.5 Å) and Hβ (pore diameter ∼ 6−7 Å), were used as the host materials. The microsecond-scale lifetime is observed for ZnO clusters confined in HZSM-5 and Hβ at room temperature. The ZnO clusters with long luminescence lifetime can be achieved by controlling the amount of ZnO clusters in zeolites.

Experimental Section

1. Sample Preparation. ZnO clusters encapsulated in zeolites were prepared by the incipient wetness impregnation method. Two types of microporous zeolites commercially available, HZSM-5 and Hβ, were used as the host materials. The zeolite of HZSM-5 has a three-dimensional pore system consisting of sinusoidal 10-ring channels (5.1 Å × 5.5 Å) and intersecting straight 10-ring channels (5.3 Å × 5.6 Å). The zeolite of Hβ has a three-dimensional pore system consisting of straight 12-ring channels (7.3 Å × 6.0 Å) and intersecting, distorted 12-ring channels (5.6 Å × 5.6 Å). HZSM-5 was obtained by calcining NH_4ZSM-5 (CBV 8014, Zeolyst International, $SiO_2/Al_2O_3 = 80$) at 550 °C for 5 h. Hβ (Nankai University, $SiO_2/Al_2O_3 = 25$) was also calcined at 550 °C for 5 h. The synthesis details are described elsewhere.[25] A given volume (the maximum adsorption volume for 1.00 g of zeolite powder) of $Zn(NO_3)_2$ aqueous solution was added into 1.00 g of zeolite powder under continuous stirring. This mixture was held for 1 h, and then it was stirred until dried at about 100 °C with a hot water bath. After this powder was kept at 120 °C for overnight, it was calcined at 550 °C for 5 h. Thus, ZnO/zeolite material was obtained. In order to achieve different ZnO loadings, the concentration of $Zn(NO_3)_2$ aqueous solution was adjusted. Two types of SiO_2 powders with different BET surfaces were used as the supports. One is denoted as SiO_2-I, with a BET surface

* Corresponding author. Tel: +86-411-84379070. Fax: +86-411-84694447. E-mail: canli@dicp.ac.cn. Home page: http://www.canli.dicp.ac.cn.

10.1021/jp060439z CCC: $33.50
Published on Web 12/07/2006

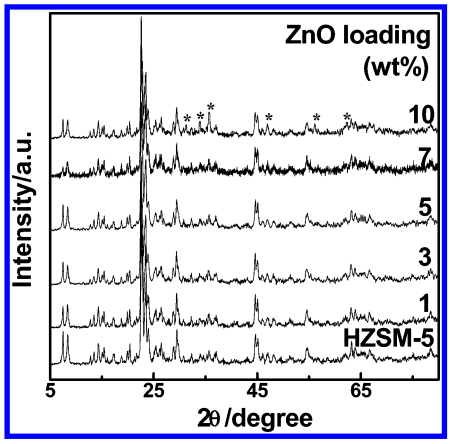

Figure 1. XRD patterns of ZnO/HZSM-5 with different ZnO loadings. The asterisks show the diffraction peaks of ZnO crystal with wurtzite structure.

area 6.0 m^2/g; the other is denoted as SiO_2-II, with a BET surface area 359 m^2/g. The preparation processes of ZnO/SiO_2 samples with different ZnO loadings were the same as that for ZnO/zeolite samples.

2. Spectroscopy Measurement. The steady-state and time-resolved photoluminescence spectra were recorded on a 32-cm monochromator (Jobin-Yvon Triax 320) with two spectral channels connecting to CCD (Jobin-Yvon Spectrum One CCD 3000) and PMT (R928). CCD detector was used to record the steady-state spectra. The time-resolved decay signal was detected by PMT and then was recorded on a Tektronix TDS 5104 oscilloscope with signal averaging of 100 flashes at 1 Hz. Prior to the experiments, the wavelength calibration of this setup was made using a mercury lamp. Two continuous wave lasers, a He−Cd laser (λ = 325 nm) and a frequency-doubled Ar ion laser (λ = 244 nm), were used as the excitation sources for steady-state spectrum measurement. The pulse excitation source for the measurements of time-resolved spectrum was the third (355 nm, ≈2 mJ/cm^2) and fourth (266 nm, ≈2 mJ/cm^2) harmonic lines of a Q-switched Nd:YAG laser (pulse width ≤20 ns). In the TRPL experiment, the detection wavelength is located in the center of luminescence band in the steady-state spectra. The decay curves obtained from TRPL measurement are the convolution of laser pulse with the impulse response of the sample.

3. X-ray Diffraction and UV−Visible Absorption Measurements. The powder X-ray diffraction (XRD) patterns of the ZnO/zeolite samples were recorded on a Rigaku MiniFlex diffractometer with Cu Kα radiation source. The 2θ range is 5−80° at a step size of 0.02° and a scanning speed of 5°/min. UV−visible absorption spectra were recorded on a JASCO V-550 spectrophotometer equipped with an integrating sphere.

Results

1. The XRD and UV−Visible Absorption Characteristics of ZnO Clusters in Zeolites. Figure 1shows the XRD patterns of ZnO/HZSM-5 with different ZnO loadings. All samples display strong diffraction peaks due to the zeolite crystal structure of HZSM-5, but the diffraction peaks of ZnO are only observed when the ZnO loading is higher than 7 wt %. The invisibility of the ZnO diffraction peaks indicates that ZnO has been highly dispersed on the surface of the support.[26−27] It is well-known that the total surface area of micropores zeolites is mainly composed of the internal surface area (wall of cages and channels) of zeolite. Therefore, ZnO has been dispersed into the pores of HZSM-5 at low ZnO loadings, and some

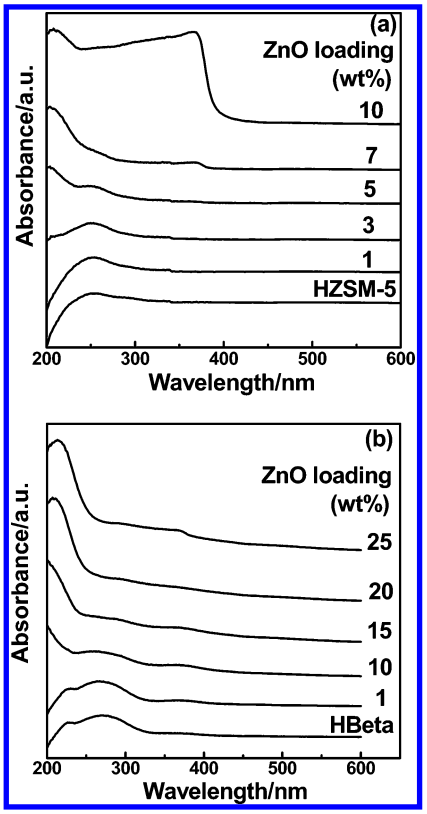

Figure 2. UV−visible absorption spectra of ZnO/zeolites with different ZnO loadings: (a) ZnO/HZSM-5 and (b) ZnO/Hβ.

macrocrystalline ZnO forms on the external surface of HZSM-5 when increasing the loading of ZnO up to 10 wt %. Figure 2a is the UV−visible absorption spectra of ZnO/HZSM-5 with different ZnO loadings. With the increase of ZnO loading, the absorption band related to HZSM-5 is weakened and the absorption band with the onset wavelength at about 265 nm is strengthened, which is ascribed to the ZnO clusters confined in the pores of HZSM-5.[25] It was reported that Zn^{2+} compensation cations in zeolite display an absorption band with wavelength smaller than about 240 nm.[23] In our case, the content of Zn^{2+} compensation cations in HZSM-5 is rather low compared with that of ZnO clusters in HZSM-5 due to the high Si/Al ratio of HZSM-5 (SiO_2/Al_2O_3 = 80); therefore, the contribution of Zn^{2+} compensation cations on this absorption band is negligible. When the ZnO loading exceeds 7 wt %, the absorption of macrocrystalline ZnO at about 370 nm is detected. Both of the XRD and UV−visible absorption results indicate that the 7 wt % loading is a critical threshold of ZnO dispersion on HZSM-5. When ZnO loading is less than the critical threshold, ZnO is dispersed into the pores of HZSM-5 to form the ZnO clusters. Once ZnO loading exceeds the critical threshold, the excessive ZnO is distributed in macrocrystalline form on the external surface of HZSM-5. Kazansky et al. reported that the zinc forms introduced in ZSM-5 by incipient wetness impregnation could be either encapsulated in the micropores of the zeolite as zinc oxide clusters or be localized on the external surface of the zeolite grains as larger particles.[28] Considering the pore texture of HZSM-5, it is reasonable to deduce that the subnanometric ZnO clusters are achieved by confining ZnO in the pore of HZSM-5.

In contrast with ZnO/HZSM-5, ZnO/Hβ samples with different ZnO loadings do not exhibit diffraction peaks of ZnO with Wurtzite structure even for ZnO loading up to 25 wt %. Figure 2b gives the UV−visible absorption spectra of ZnO/Hβ

TABLE 1: Compositions of ZnO/Zeolites Samples

sample	composition of ZnO per unit cell [$(ZnO)_x$ zeolites][a]	wt % of ZnO
HZSM-5 ($SiO_2/Al_2O_3 = 80$)	$H_n[(AlO_2)_n(SiO_2)_{96-n}]$[b]	
ZnO/HZSM-5	$(ZnO)_{0.7}$HZSM-5	1
	$(ZnO)_{2.2}$HZSM-5	3
	$(ZnO)_{3.7}$HZSM-5	5
	$(ZnO)_{5.4}$HZSM-5	7
	$(ZnO)_{8.0}$HZSM-5	10
Hβ ($SiO_2/Al_2O_3 = 25$)	$H_n[(AlO_2)_n(SiO_2)_{64-n}]$[b]	
ZnO/Hβ	$(ZnO)_{0.5}$Hβ	1
	$(ZnO)_{5.3}$Hβ	10
	$(ZnO)_{8.4}$Hβ	15
	$(ZnO)_{12.0}$Hβ	20
	$(ZnO)_{16.0}$Hβ	25

[a] x denotes the molecular numbers of ZnO per unit cell of zeolite. [b] n denotes the Al atom numbers per unit cell of zeolite.

with different ZnO loadings. All samples display the absorption band with onset wavelength at about 265 nm related to subnanometric ZnO clusters, and a weak absorption band at about 370 nm related to macrocrystalline ZnO is observed for 25 wt % ZnO/Hβ. That is, ZnO clusters can be accommodated in the pores of Hβ even for the loading of ZnO up to 25 wt %. The difference of ZnO dispersion capacities between HZSM-5 and Hβ is reasonable considering their different pore texture. The larger pore dimension exists in Hβ than that in HZSM-5; thus, the higher dispersion capacities of ZnO clusters exist in Hβ zeolite.

Table 1 gives the compositions of ZnO/zeolites samples. It demonstrates the ZnO loading densities (molecular numbers of ZnO per unit cell of zeolite) of different ZnO/zeolites samples. The dispersion capacity of ZnO clusters in HZSM-5 and Hβ is 7 wt % ZnO loading for HZSM-5 and 25 wt % ZnO loading for Hβ, which corresponds to 5.4 ZnO molecules per unit cell of HZSM-5 and 16 ZnO molecules per unit cell of Hβ, respectively. For the 10 wt % ZnO/HZSM-5 sample, the excessive ZnO forms the macrocrystalline ZnO on the external surface of HZSM-5 zeolite.

2. The Steady-State Photoluminescence Characteristics of ZnO/Zeolites. The 244- and 325-nm laser lines are used to detect the steady-state PL spectra of ZnO/zeolites samples, and the 266- and 355-nm laser lines are used to detect the dynamic process of ZnO/zeolites samples in the TRPL experiment. On the basis of the UV−visible absorption spectra, the excitation wavelength of 244 or 266 nm locates in the absorption band of ZnO clusters confined in zeolites, whereas the excitation wavelength of 325 or 355 nm is out of the absorption band of ZnO clusters but inside the absorption region of macrocrystalline ZnO. This means that the spectra excited by 244 and 266 nm can give the information about ZnO clusters inside of zeolites and macrocrystalline ZnO outside of zeolites, whereas the spectra excited by 325 and 355 nm mainly present the information about macrocrystalline ZnO outside of zeolites.

In our previous work,[29] it has been reported that the visible luminescence from bulk ZnO is associated with the oxygen vacancies in ZnO, and the electronic states responsible for the visible luminescence bands are changing with the density of oxygen vacancies in ZnO. The green (centered at ca. 520 nm), yellow (centered at ca. 580 nm), and orange (centered at ca. 640 nm) luminescence bands are ascribed to the state of ZnO with high density of oxygen vacancies, with moderate density of oxygen vacancies, and with less oxygen vacancies, respectively. The subnanometric ZnO clusters confined in zeolites display the purple luminescence band centered at about 440 nm,

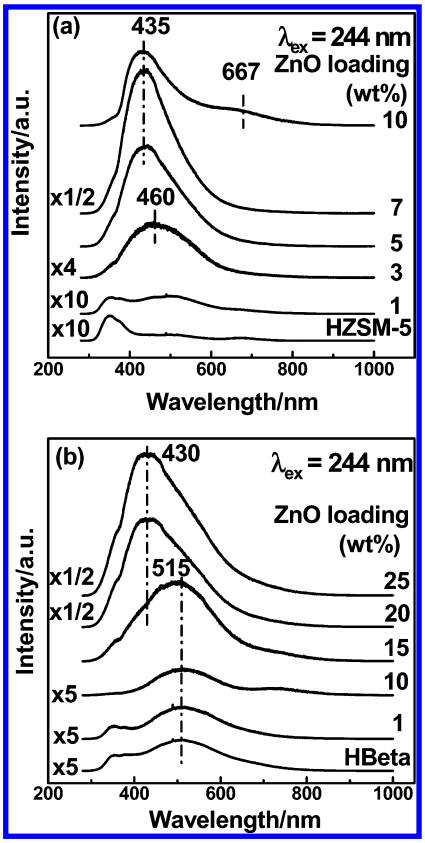

Figure 3. Steady-state photoluminescence spectra of ZnO/zeolites with different ZnO loadings: (a) ZnO/HZSM-5 and (b) ZnO/Hβ, excited at 244 nm.

which is ascribed to the coordinatively unsaturated Zn sites with oxygen vacancies in subnanometric ZnO clusters.[25] The purple luminescence band ascribed to ZnO clusters has higher quantum efficiency than that of the visible luminescence bands ascribed to the macrocrystalline ZnO.

Figure 3a shows the steady-state PL spectra of ZnO/HZSM-5 excited by 244 nm. The purple luminescence band related to subnanometric ZnO clusters is observed for ZnO/HZSM-5 with different ZnO loadings. The intensity of this band increases significantly when increasing ZnO loading up to 7 wt %, while the position of this band shifts from 460 nm for 3 wt % ZnO/HZSM-5 sample to 435 nm for higher ZnO loading samples. In addition, the ZnO/HZSM-5 with 10 wt % ZnO loading displays a weak orange luminescence band (centered at 667 nm) related to macrocrystalline ZnO. In the steady-state PL spectra of ZnO/HZSM-5 excited by 325 nm, all samples display the green and orange luminescence bands related to macrocrystalline ZnO, and the purple luminescence band is not observed.[25] Figure 3b is the steady-state PL spectra of ZnO/Hβ excited by 244 nm. The purple luminescence band appears when ZnO loading reaches 15 wt % and its intensity increases when further increasing the ZnO loading up to 25 wt %, while the visible luminescence bands ascribed to macrocrystalline ZnO are not observed in the steady-state PL spectra of ZnO/Hβ samples excited by 244 and 325 nm.

The maximum intensity of purple luminescence band appears for ZnO/HZSM-5 at 7 wt % ZnO loading (5.4 ZnO molecules per unit cell) and for ZnO/Hβ at 25 wt % ZnO loading (16 ZnO molecules per unit cell). This is consistent with the dispersion capacities (the critical threshold) of ZnO clusters in HZSM-5 and in Hβ. The absence of the visible luminescence band for ZnO/Hβ is due to the larger dispersion capacities of

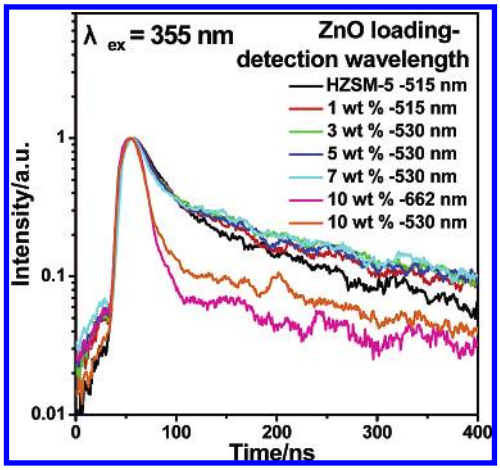

Figure 4. TRPL spectra of ZnO/HZSM-5 with different ZnO loadings, excited at 355 nm. The ZnO loadings and the detection wavelength are marked.

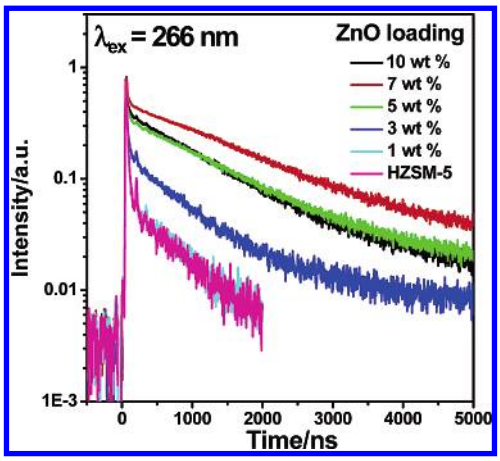

Figure 5. TRPL spectra of ZnO/HZSM-5 with different ZnO loadings detected at 435 nm, excited at 266 nm.

ZnO clusters in Hβ, and no macrocrystalline ZnO is formed on the external surface of the Hβ zeolite.

3. Time-Resolved Photoluminescence Characteristics of ZnO/Zeolites. Figure 4 shows the wavelength-dependent TRPL spectra of ZnO/HZSM-5 with different ZnO loadings excited by 355 nm. The visible luminescence bands centered at 515, 530, and 662 nm decay rapidly, on nanosecond scale. Many researchers have reported the lifetime of visible luminescence bands, which heavily depends on the ZnO forms and preparation methods.[7−12,16] Bauer and co-worker detected a lifetime shorter than 400 ps for a nanocrystalline ZnO thin film,[7] Millers et al. observed about 100 ns lifetime for ZnO nanopowder,[8] a lifetime of several tens to thousands of nanoseconds had been reported by other workers for ZnO colloids,[9−12] and a lifetime of several millisecond appeared for nanosized ZnO included in MCM-41.[16] For the macrocrystalline ZnO outside of HZSM-5, the lifetimes of visible luminescence bands are several tens of nanoseconds, which are in the region of instrument response.

Figure 5 gives the dynamic decay curves of ZnO clusters confined in HZSM-5 excited by 266 nm, which is significantly different from the decay process of macrocrystal ZnO outside of HZSM-5. These decay curves are fit by the nonlinear least-squares method to the double exponential decay law as given by the expression

$$y = A_1 \exp(-x/t_1) + A_2 \exp(-x/t_2) \quad (1)$$

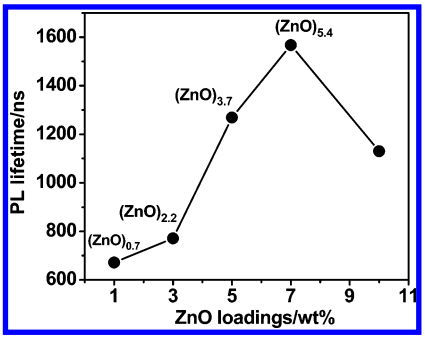

Figure 6. The lifetime (slow component in microsecond scale) of ZnO/HZSM-5 vs the dispersion amount of ZnO in HZSM-5. The molecular numbers of ZnO per unit cell of HZSM-5 are labeled.

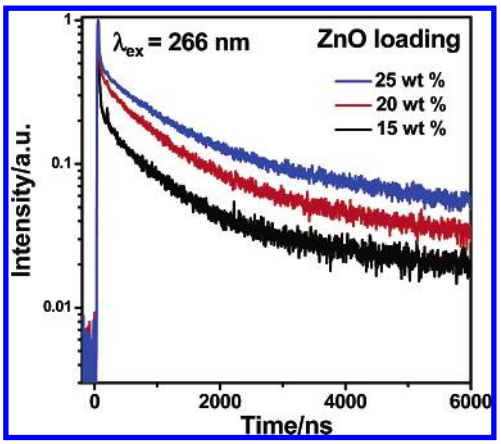

Figure 7. TRPL spectra of ZnO/Hβ with different ZnO loadings detected at 430 nm, excited at 266 nm.

The faster of the two decay components has a time constant $\tau \approx 20$ ns, which is within the instrument response region. The slow component on the microsecond scale is quite sensitive to the ZnO loadings in HZSM-5. Figure 6 shows the correlation between the lifetime determined from the slow component and the ZnO loadings. With the increase of the ZnO loading, the lifetime continuously increases till 7 wt % ZnO loading (5.4 ZnO molecules per unit cell of HZSM-5) is reached. When the ZnO loading exceeds this value, the corresponding luminescence lifetime declines again. Changing the detection wavelength from 435 to 667 nm for 10 wt % ZnO/HZSM-5 sample, the orange luminescence band decays rapidly on the nanosecond scale, which is similar to that shown in Figure 4.

The microsecond lifetimes are also observed for ZnO/Hβ samples in Figure 7 excited by 266 nm. These dynamic curves display multiexponential decay detected at 430 nm, and the lifetime of ZnO clusters also correlates with the ZnO loadings in Hβ. The lifetime increases gradually with the increase of ZnO loadings till 25 wt % ZnO loading (16 ZnO molecules per Hβ unit cell).

Discussion

As the semiconductor particle size decreases, its optical properties, such as band gap and photoluminescence lifetime, are usually changed due to the quantum effect.[30−32] The subnanometric ZnO clusters confined in micropore zeolites are well within the quantum confinement regime and these ZnO clusters display significantly different optical behaviors from bulk material, for example, the appearance of purple luminescence (Figure 3) and the microsecond lifetime at room temperature (Figures 5 and 7). It is also reported that as the

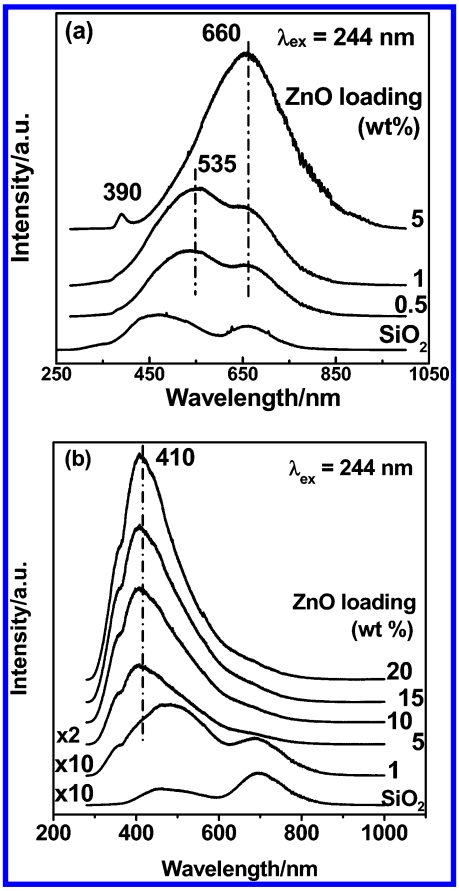

Figure 8. Steady-state photoluminescence spectra of ZnO/SiO_2 with different ZnO loadings: (a) ZnO/SiO_2-I and (b) ZnO/SiO_2-II, excited at 244 nm.

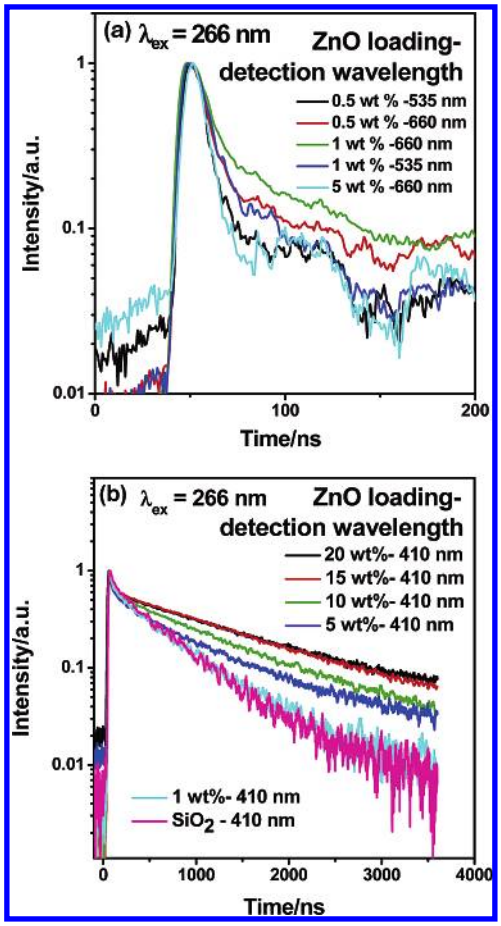

Figure 9. TRPL spectra of ZnO/SiO_2 with different ZnO loadings: (a) ZnO/SiO_2-I and (b) ZnO/SiO_2-II, excited at 266 nm. The ZnO loadings and the detection wavelength are marked.

semiconductor cluster size decreases, although the optical absorption still shows the characteristics of the semiconductor itself, the excited-state relaxation dynamics is gradually dominated by the interface and host.[33] In general, the PL decay rate is the sum of the radiative and nonradiative decay rates: $\tau_{PL}^{-1} = \tau_r^{-1} + \tau_{nr}^{-1}$, where τ_{PL}, τ_r, and τ_{nr} are PL, radiative, and nonradiative decay time constants, respectively. At room temperature, the PL decay rate is dominated by the τ_{nr}^{-1} due to the activation of nonradiative centers.[9] For the ZnO clusters confined in zeolites, the interface and host (zeolite) may play an important role in the nonradiative relaxation because of the large surface-to-volume ratio of ZnO clusters. There are strong interactions between ZnO clusters and zeolite host via the coordination of zinc atoms of ZnO clusters with the zeolite framework oxygen atoms, which have been proved by UV Raman spectra.[25] The large Stokes-shifted and emission spectral broadening also indicate the existence of strong electron−phonon interaction between ZnO clusters and zeolites lattice. The similar coupling of electronic transition to surface and host phonons has been reported for CdS superclusters inside zeolites, and the interface and host (zeolite) phonons were mainly responsible for the radiationless relaxation processes.[33] In the following text, the decay processes of ZnO/zeolites will be discussed by the theories of multiphonon nonradiative transitions, which have been successfully used to explain the relaxation of CdS superclusters in zeolites,[33,34] CdS colloidal particles,[35] ion in crystals,[36] etc.

The theory of multiphonon nonradiative transitions describes the nonradiative relaxation of an electronic state stimulated by the excitation and emission of mediating phonons.[37] The rate of a nonradiative electron transfer, k_{nr}, at all temperatures is given as[38]

$$k_{nr} = \frac{2\pi}{\hbar}|V_{ab}(R)|^2 \exp[-S(2\bar{\nu}+1)] I_p(2S[\bar{\nu}(\bar{\nu}+1)]^{1/2}) \times [(\bar{\nu}+1)/\bar{\nu}]^{p/2} \quad (2)$$

where $\bar{\nu}$ is the Bose thermal occupation of phonon mode $\hbar\omega$, p is the exothermicity expressed as integral number of vibrational quanta, I_p is a modified Bessel function, and S (Huang−Rhys factor) is the Franck−Condon phonon displacement parameter. The Huang−Rhys parameter S, reflecting the strength of electron−phonon interactions, can be estimated from the experimentally measured luminescence spectrum. The half-width of emission spectrum can be simulated by[37]

$$W_h = 4(\ln 2)^{1/2}(kTS\overline{\hbar\omega})^{1/2} \quad (3)$$

where S is the Huang−Rhys parameter, k is the Boltzman constant, T is temperature, and $\overline{\hbar\omega}$ is the average energy of mediating phonons with frequency ω.

For ZnO/HZSM-5 samples, increasing the ZnO loadings from 3 to 7 wt %, the half-width of purple luminescence band (estimated from the Gaussian fitting of curves) reduced from 150 to 120 nm, as shown in Figure 3a. The S values estimated from eq 3 are also decreased with the increase of ZnO loadings, which means the weakening of electron−phonon interaction between ZnO clusters and zeolites lattice. On the other hand, the emerging of the bathochromic shift in the absorption onset of ZnO clusters (Figure 2a) indicates the occurrence of interac-

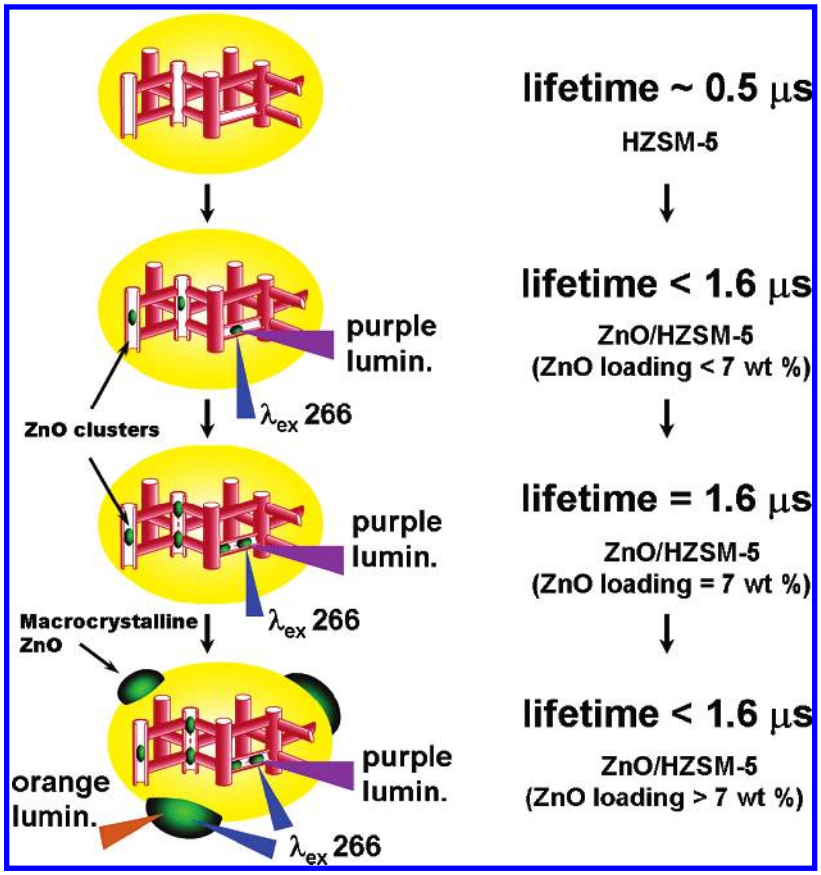

Figure 10. Schematic illustration of the lifetime evolution of ZnO clusters confined in HZSM-5 with the increase of ZnO loadings.

tions between these ZnO clusters with the increase of the molecular numbers of ZnO per unit cell. That is, with the increase of ZnO loadings, the interaction between ZnO clusters and zeolite lattice is weakened and the interaction between ZnO clusters confined in HZSM-5 is strengthened. Therefore, the nonradiative processes dominated by host phonons are inhibited and the nonradiative decay rate, k_{nr}, is reduced with the increase of ZnO loadings. Accordingly, the emission lifetime of ZnO clusters increases gradually with the increase of ZnO loadings, as shown in Figure 6. When increasing ZnO loading to 10 wt %, which is higher than the dispersion capacities (7 wt %) of ZnO clusters confined in HZSM-5, the amount of ZnO clusters confined in HZSM-5 is not increased, but macrocrystalline ZnO forms on the external surface of HZSM-5. As shown in Figure 6, the luminescence lifetime of 10 wt % ZnO/HZSM-5 declines comparing with that of 7 wt % ZnO/HZSM-5. It is deduced that the decrease of the lifetime is related to macrocrystalline ZnO on the external surface of HZSM-5, the further reasons would be investigated in the following work. The similar discussion should be applicable to ZnO/Hβ samples with different ZnO loadings. With the increase of ZnO loadings, the half-width of purple luminescence band is declined, the coupling of electronic transition to zeolite host phonons is weakened, and the corresponding nonradiative decay rate, k_{nr}, is decreased. Therefore, the lifetime of ZnO clusters increases with the increase of ZnO loadings till 25 wt % ZnO loading (16 ZnO molecules per unit cell of Hβ).

We also prepared ZnO/SiO_2 samples with different ZnO loadings for comparison. Figure 8 shows the steady-state PL spectra of ZnO/SiO_2 samples excited by 244 nm. For 5 wt % ZnO/SiO_2-I sample, the orange luminescence band centered at 660 nm is observed beside the exciton emission band centered at 390 nm in Figure 8a, but for ZnO/SiO_2-II samples with different ZnO loadings, the purple luminescence band centered at 410 nm is observed in Figure 8b. The TRPL spectra of these samples also show significantly different character in Figure 9 excited by 266 nm. The visible luminescence bands of ZnO/SiO_2-I samples decay rapidly in nanosecond magnitude (Figure 9a), which is similar to the results of macrocrystalline ZnO outside of HZSM-5 excited by 355 nm, but the ZnO/SiO_2-II samples display long luminescence lifetimes in microsecond magnitude (Figure 9b), which is similar to the results of ZnO clusters confined in the channels of HZSM-5. The BET surface area of SiO_2-I powder is 6.0 m^2/g; namely, ZnO clusters cannot form in this support due to the lack of the pores' structure. Hence, the luminescence properties of ZnO/SiO_2-I are similar to those of macrocrystalline ZnO. The SiO_2-II support possesses a large BET surface area (359 m^2/g) and its porous structure consists of ~5.3 Å micropores and ~100 Å mesopores (Supporting Information). In the UV−visible absorption spectra of ZnO/SiO_2-II, an absorption band with onset wavelength at about 250 nm is observed and no macrocrystalline ZnO absorption appears even for ZnO loading up to 20 wt % (Supporting Information). On the basis of the pore distribution of SiO_2-II and the UV−visible absorption spectra of ZnO/SiO_2-II, it is deduced that subnanometric ZnO clusters are highly dispersed in the porous SiO_2-II support. Therefore, these ZnO clusters display the similar luminescence properties with that of ZnO clusters confined in HZSM-5.

The scheme for the lifetime evolution of ZnO clusters confined in HZSM-5 with the increase of ZnO loadings is illustrated in Figure 10. At low ZnO loadings, the lifetimes of ZnO clusters confined in HY are several hundreds of nanoseconds due to the strong electron−phonon interactions between ZnO clusters and zeolite lattice. With the increase of ZnO loadings, the interactions between these ZnO clusters occur and

the coupling of electronic transition to host phonons is weakened, as a result, the lifetimes gradually increase up to the microsecond magnitude. The higher ZnO loading leads to macrocrystalline ZnO formed on the external surface of HZSM-5, and the luminescence lifetime declines again.

Conclusions

In this paper, we studied the dynamics of ZnO clusters confined in different zeolite micropore hosts by TRPL spectroscopy. The subnanometric ZnO clusters display significantly different optical behaviors from macrocrystalline ZnO, mainly due to the quantum confinement effect. Besides the blue-shift of absorption edge and the purple luminescence band with high quantum efficiency, the ZnO clusters exhibit the microsecond-scale emission lifetime at room temperature. The lifetime is related to the dispersion amount of ZnO clusters in zeolites, and the microsecond lifetime is observed for ZnO/HZSM-5 and ZnO/Hβ. The TRPL results are discussed in terms of the theory of multiphonon-induced radiationless transitions. The lifetime of ZnO clusters is significantly affected by the electron−phonon interaction between ZnO clusters and zeolite host. ZnO clusters with long-lifetime luminescence can be achieved by controlling ZnO loadings and reducing the coupling of electronic transition to host phonons. The similar long-lived luminescence is obtained when dispersing ZnO clusters into porous SiO_2. It is suggested that encapsulating the semiconductor clusters in the porous supports is a possible way to inhibit or to retard the electron−hole recombination in semiconductors.

Acknowledgment. This work was financially supported by the National Science Foundation of China (NSFC, grant 20373069 and 20273069), the National Basic Research Program of China (grant 2003CB615806), and the Knowledge Innovation Program of Chinese Academy of Science (DICP K2006E2).

Supporting Information Available: The pore distributions of SiO_2-II support and the UV-visible absorption spectroscopy of ZnO/SiO_2-II with different ZnO loadings, as described in the text. This material is available free of charge via the Internet at http://pubs.acs.org.

References and Notes

(1) Hoffmann, M. R.; Martin, S. T.; Choi, W.; Bahnemann, D. W. *Chem. Rev.* **1995**, *95*, 69.
(2) O'Regan, B.; Grätzel, M. *Nature (London)* **1991**, *353*, 737.
(3) Hagfeldt, A.; Grätzel, M. *Acc. Chem. Res.* **2000**, *33*, 269.
(4) Kim, S. W.; Ueda, M.; Kotani, T.; Fujita, S.; Fujita, S. *Jpn. J. Appl. Phys.* **2003**, *42*, L568.
(5) Huang, M.; Mao, S.; Feick, H.; Yan, H.; Wu, Y.; Kind, H.; Weber, E.; Russo, R.; Yang, P. *Science* **2001**, *292*, 1897.
(6) Birkmire, R. W. *Solar Energy Mat. Solar Cells* **2001**, *65*, 17.
(7) Bauer, C.; Boschloo, G.; Mukhtar, E.; Hagfeldt, A. *Chem. Phys. Lett.* **2004**, *387*, 176.
(8) Millers, D.; Grigorjeva, L.; Łojkowski, W.; Strachowski, T. *Radiat. Meas.* **2004**, *38*, 589.
(9) van Dijken, A.; Meulenkamp, E. A.; Vanmaekelbergh, D.; Meijerink, A. *J. Phys. Chem. B* **2000**, *104*, 1715.
(10) Koch, U.; Fojtik, A.; Weller, H.; Henglein, A. *Chem. Phys. Lett.* **1985**, *122*, 507.
(11) Bahnemann, D. W.; Kormann, C.; Hoffmann, M. R. *J. Phys. Chem.* **1987**, *91*, 3789.
(12) Kamat, P. V.; Patrick, B. *J. Phys. Chem.* **1992**, *96*, 6829.
(13) Hong, S.; Joo, T.; Park, W. I.; Jun, Y. H.; Yi, G. C. *Appl. Phys. Lett.* **2003**, *83*, 4157.
(14) Kwok, W. M.; Djurišić, A. B.; Leung, Y. H.; Chan, W. K.; Phillips, D. L. *Appl. Phys. Lett.* **2005**, *87*, 093108.
(15) Travnikov, V. V.; Freiberg, A.; Savikhin, S. F. *J. Lumin.* **1990**, *47*, 107.
(16) Tang, G. Q.; Xiong, Y.; Zhang, L. Z.; Zhang, G. L. *Chem. Phys. Lett.* **2004**, *395*, 97.
(17) Stucky, G. D.; Dougall, J. E. M. *Science* **1990**, *247*, 669.
(18) Ozin, G. A. *Adv. Mater.* **1992**, *4*, 612.
(19) Meneau, F.; Sankar, G.; Morgante, N.; Cristol, S.; Catlow, C. R. A.; Thomas, J. M.; Greaves, G. N. *Nucl. Instrum. Methods Phys. Res., Sect. B* **2003**, *199*, 499.
(20) Jeong, N. C.; Kim, H. S.; Yoon, K. B. *Langmuir* **2005**, *21*, 6038.
(21) Seifert, R.; Kunzmann, A.; Calzaferri, G. *Angew. Chem., Int. Ed.* **1998**, *37*, 1521.
(22) Brühwiler, D.; Seifert, R.; Calzaferri, G. *J. Phys. Chem. B* **1999**, *103*, 6397.
(23) Wark, M.; Kessler, H.; Schulz-Ekloff, G. *Microporous Mater.* **1997**, *8*, 241.
(24) Readman, J. E.; Gameson, I.; Hriljac, J. A.; Edwards, P. P.; Anderson, P. A. *Chem. Commun.* **2000**, 595.
(25) Chen, J.; Feng, Z. C.; Ying, P. L.; Li, C. *J. Phys. Chem. B* **2004**, *108*, 12669.
(26) Xie, Y. C.; Tang, Y. Q. *Adv. Catal.* **1990**, *37*, 1.
(27) Xiao, F. S.; Xu, W.; Qiu, S.; Xu, R. *J. Mater. Chem.* **1994**, *4*, 735.
(28) Kazansky, V. B; Borovkov, V. Yu.; Serikh, A. I.; van Santen, R. A.; Anderson, B. G. *Catal. Lett.* **2000**, *66*, 39.
(29) Chen, J.; Feng, Z. C.; Ying, P. L.; Li, M. J.; Han, B.; Li, C. *Phys. Chem. Chem. Phys.* **2004**, *6*, 4473.
(30) Miller, R. C.; Kleinman, D. A.; Tsang, W. T.; Gossard, A. C. *Phys. Rev. B* **1981**, *24*, 1134.
(31) (a) Rossetti, R.; Nakahara, S.; Brus, L. E. *J. Chem. Phys.* **1983**, *79*, 1086. (b) Brus, L. E. *J. Chem. Phys.* **1984**, *80*, 4403.
(32) Mittleman, D. M.; Schoenlein, R. W.; Shiang, J. J.; Colvin, V. L.; Alivisatos, A. P.; Shank, C. V. *Phys. Rev. B* **1994**, *49*, 14435.
(33) Wang, Y.; Herron, N. *J. Phys. Chem.* **1988**, *92*, 4988.
(34) Chen, W.; Wang, Z. G.; Lin, Z. J.; Lin, L. Y. *Solid State Commun.* **1997**, *101*, 371.
(35) Chestnoy, N.; Harris, T. D.; Hull, R.; Brus, L. E. *J. Phys. Chem.* **1986**, *90*, 3393.
(36) Fong, F. K. *Theory of Molecular Relaxation. Applications in Chemistry and Biology*; Wiley: New York, 1975.
(37) Huang, K. *Prog. Phys.* **1981**, *1*, 31.
(38) Jortner, J. *J. Chem. Phys.* **1976**, *64*, 4860.